# Interface driven magnetoelectric effects in granular $CrO_2$

A. Bajpai[1], P. Borisov[2], S. Gorantla[1], R. Klingeler[3,1], J. Thomas[1], T. Gemming[1], W. Kleemann[2] and B. Büchner[1]

[1] *Leibniz-Institute for Solid State and Materials Research, IFW Dresden, 01171 Dresden, Germany*
[2] *Angewandte Physik, Universität Duisburg-Essen, 47048 Duisburg, Germany*
[3] *Kirchhoff-Institute for Physics, Universität Heidelberg, 69120 Heidelberg, Germany*

arXiv:1008.0113v1 [cond-mat.str-el] 31 Jul 2010

PACS `75.85.+t` – Magnetoelectric effects, multiferroics
PACS `85.75.-d` – Magnetoelectronics; spintronics: devices exploiting spin polarized transport or integrated magnetic fields
PACS `72.25.Mk` – Spin transport through interfaces

**Abstract.** - Antiferromagnetic and magnetoelectric $Cr_2O_3$-surfaces strongly affect the electronic properties in half metallic $CrO_2$. We show the presence of a $Cr_2O_3$ surface layer on $CrO_2$ grains by high-resolution transmission electron microscopy. The effect of these surface layers is demonstrated by measurements of the temperature variation of the magnetoelectric susceptibility. A major observation is a sign change at about 100 K followed by a monotonic rise as a function of temperature. These electric field induced moments in $CrO_2$ are correlated with the magnetoelectric susceptibility of pure $Cr_2O_3$. This study indicates that it is important to take into account the magnetoelectric character of thin surface layers of $Cr_2O_3$ in granular $CrO_2$ for better understanding the transport mechanism in this system. The observation of a finite magnetoelectric susceptibility near room temperature may find utility in device applications.

**Introduction.** – Advances in the field of spintronics are driven by the identification of materials with high degree of spin polarization (such as half metalic ferromagnets) and materials in which magnetism can be tuned not only with an applied magnetic field but also through an applied electric field ( magnetoelectric materials) [1–4]. This in turn has lead to the study of composites of ferromagnetic and ferroelectric materials, which can exhibit properties superior to a single-phase compound [3].

A potential candidate for spintronic applications is $CrO_2$, which is a well established half metallic ferromagnet ($T_C \approx 393\,K$) [5–8]. Owing to the large spin polarization value as well as it being a room temperature ferromagnet, $CrO_2$ is widely explored, both in thin films [7–12] and in bulk [13–15] form. A major limiting factor in realization of actual devices based on $CrO_2$ has been the issue of stability of its surface [9–15]. For instance, it easily converts to other stable oxides, such as $Cr_2O_3$. However, in case of granular $CrO_2$, it was recognised that this could be a rather advantageuos situation as far as magnetoresistive properties are concerned. The presence of $Cr_2O_3$ as an insulating surface layer makes granular $CrO_2$ a natural source of a Magnetic Tunnel Junction [5, 13, 14]. This, together with the fact that $Cr_2O_3$ as the insulating surface is both antiferromagnetic (AFM) and magnetoelectric (ME) [16–22] below $T_N \approx 307\,K$ in bulk, makes granular $CrO_2$ interesting from both the fundamental as well as the technological point of view. Correspondingly, this system provides the opportunity of a high spin polarization intrinsically associated with $CrO_2$ as well as of a significant magnetoelectricity arising from the $Cr_2O_3$ surfaces.

It is emphasized that while the phenomenon of magnetoelectricity is well established for $Cr_2O_3$ in the bulk single crystalline and polycrystalline forms [16, 17, 20], these features have not been explored when $Cr_2O_3$ appear as a grain boundary in granular $CrO_2$. In this work we first confirm the presence of the crystalline surface layer of $Cr_2O_3$ by TEM investigations. Further, we present direct experimental measurement of magnetoelectric susceptibility in granular $CrO_2$ in which $Cr_2O_3$ appears as a surface layer outside the $CrO_2$ grain.

**Experimental Details.** – The sample is in the form of loosely sintered pellets of $CrO_2$, containing grains in the form of micron size rods. The synthesis and other characterization details can be found elsewhere [24]. It is important to note that these samples have shown much better magnetoresistive properties than commercial powders [25]. The transmission electron microscopic (TEM) investigation on individual $CrO_2$ grains (derived from the same pellet) was performed using a FEI Tecnai F30 S-Twin. The measurements of the ME susceptibility have been performed using a superconducting quantum interference device (SQUID), MPMS-5S from Quantum Design, by modification of its ac susceptibility option [23]. The electrical conductivity has been measured in the standard four probe geometry, using a Quantum Design PPMS.

**Results and discussions. –**

*Transmission Electron Microscopy Measurements.* For the TEM investigations, a single grain with a length of the order of a few $\mu$m and thickness of the order of 500 nm was isolated from the same pellet (Fig.1a) on which the ME susceptibility and resistivity measurements have been conducted. This sample shows a saturation magnetization of the order of 120 emu/g [24]. The TEM specimen is prepared by pressing a sparse layer of powder onto the grid and identifying isolated grains from the edges (Fig.1b). From the relatively thick grains a suitably thin edge was used for high resolution transmission electron microscopy (HRTEM). Fig.1b shows an individual $CrO_2$ grain, the arrowhead in the figure represents the region from which the HRTEM image is obtained. The $CrO_2$ grain was tilted to the $[-111]$ zone axis using Kikuchi lines prior to HRTEM imaging which is shown in Fig.1c. The Fast Fourier Transform (FFT) diffractogram from the highlighted region in Fig.1c was analyzed using the ELDISCA software [27], for determining the crystal structure. The surface layer is found to be polycrystalline $Cr_2O_3$, while no possible zone axis was found when a FFT diffractogram was analyzed with $CrO_2$ crystal structure. The presence of similar continuous $Cr_2O_3$ layers was observed along the edges of other $CrO_2$ grains.

The presence of $Cr_2O_3$ as a surface layer is consistent with the better tunneling magnetoresistance as observed in these samples [25]. Such a layer of low crystallinity has earlier been seen in TEM studies on commercial powders [14] and very recently in nanorods of $CrO_2$ [28], synthesized using our synthesis route [24]. However the direct observation of the crystalline $Cr_2O_3$ as a surface layer, such as shown in Fig.1c, is rare.

*Magnetoelectric susceptibility.* The linear ME susceptibility $\alpha_{ij}$ is defined using $\mu_0 M_i \propto \alpha_{ij} \mathrm{E}_j$ or $\mathrm{P}_j \propto \alpha_{ij} \mathrm{H}_i$,where $\mathrm{M}_i$ is the electric-field-induced magnetization and $\mathrm{P}_j$ is the magnetic-field-induced polarization [16]. In this work, we have measured electric- field-induced magnetization. Our ME susceptibility measurements are conducted by applying an ac voltage, $u(t) = u_0 \cos \omega t$ across the sample and measuring the induced ac magnetic moment, $m(t) = m' \cos \omega t + m'' \sin \omega t$ in zero external magnetic field.The schematic of the measurement, which can be done in both *constant applied voltage amplitude* ($u_0 =$ const) and *constant applied current amplitude* mode ($i_0 =$ const), is shown in Figure 2. The details of the measurement procedure can be found elsewhere [23]. The lower panel of Figure 2 shows a complex plane representation of the real (m') and the imaginary (m") part of the ME susceptibility as measured on the $CrO_2$ sample at $i_0 =$ const mode at 10 Hz.

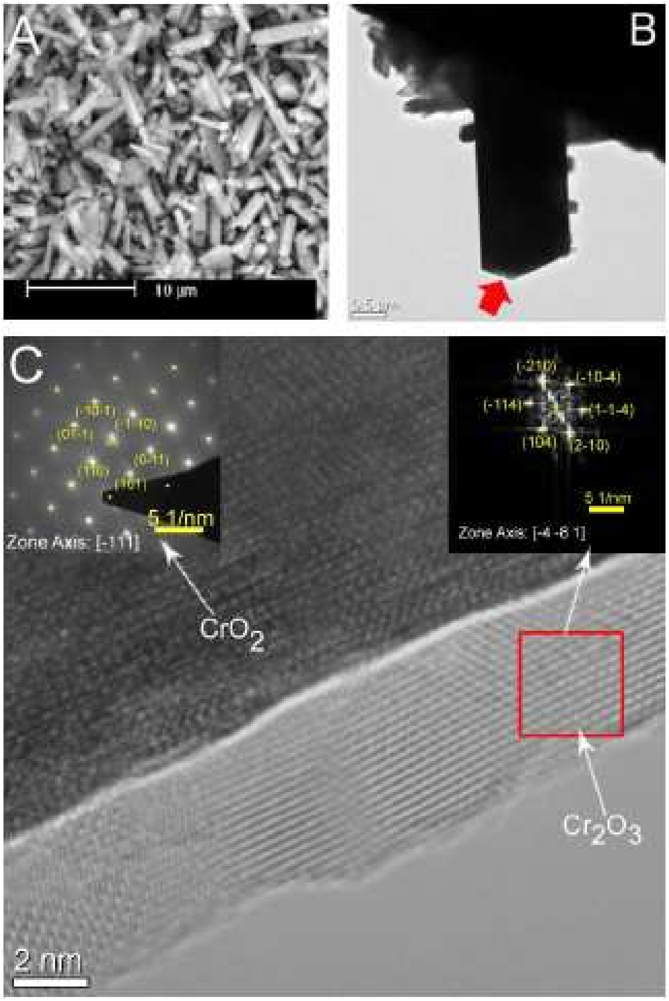

Fig. 1: (a) SEM image of a pellet containing the $CrO_2$ grains in the shape of micron size rods. The bright field TEM image of an individual $CrO_2$ grain is shown in (b). The HRTEM image of $CrO_2$ grain with $Cr_2O_3$ oxide layer is shown in (c). The right inset in (c) shows the FFT diffractogram, extracted from the region represented by the rectangular box in (c), overlaid by the calculated diffraction pattern for the [-4-8 1] zone axis of $Cr_2O_3$. The left inset shows the experimental diffraction pattern of $CrO_2$ grain overlaid by a calculated pattern for the [-111] zone axis.

Fig.3(a) shows the real part of the electric field induced moment as a function of temperature for granular $CrO_2$. The data are obtained in both cooling and heating cycles, measured in constant current amplitude mode. The moments exhibit a change of sign below 100 K, followed by a rapid rise in magnitude up to the maximum temperature of 350 K. A substantial thermal hysteresis is observed

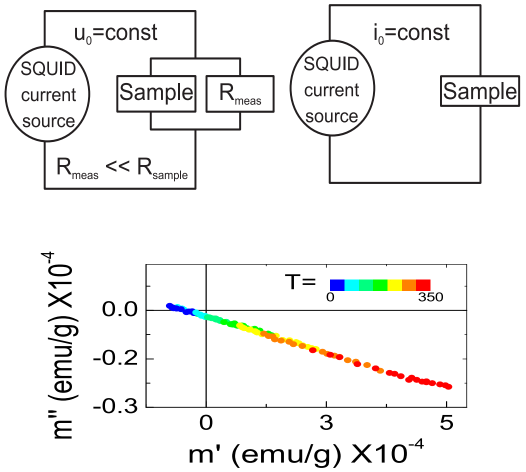

Fig. 2: The upper left panel depicts the schematic of the ME susceptibility measurement in constant voltage amplitude mode, while the upper right panel shows the same in constant current amplitude mode. The lower panel displays the complex plane representation ($m''$ vs. $m'$) of the real and the imaginary parts of the electric field induced moment as measured in granular $CrO_2$ at different temperatures.

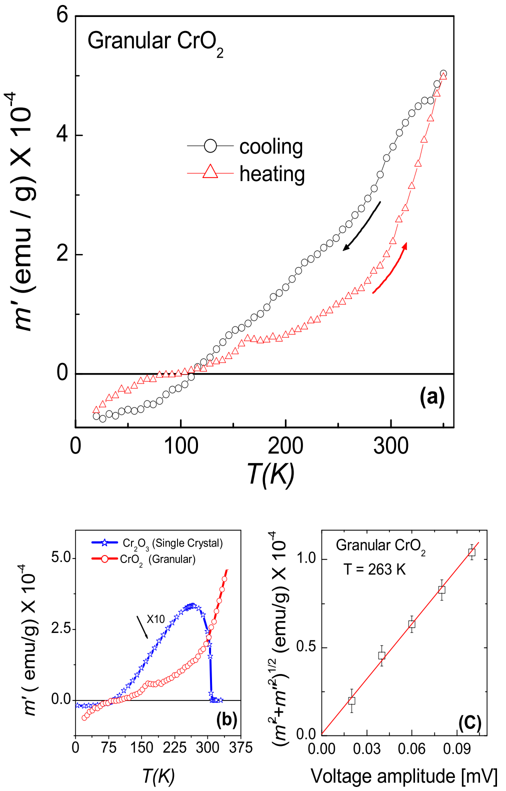

Fig. 3: (a) Temperature dependence of the real part of the electric field induced moment ($m'$) in cooling and heating cycles, showing thermal hysteresis and a change of sign around 100K. (b) $m'$ in a single crystal of $Cr_2O_3$ (blue stars) and granular $CrO_2$ (red circles). The data set on $Cr_2O_3$ is multiplied by a factor of 10. (c) Resultant amplitude of the moment varying linearly as a function of the applied electric field amplitude at 263 K.

in cooling and heating cycles, which becomes pronounced above 200 K. Fig.3(b) compares the ME susceptibility in a single crystal of $Cr_2O_3$ ( blue stars) with that measured on the granular $CrO_2$ (red circles). Both measurements were performed in heating cycle using the same experimental set up. The ac electric-field amplitude for granular $CrO_2$ and $Cr_2O_3$ were 1 V/m and 63 kV/m, respectively. In addition, the single crystal of $Cr_2O_3$ was ME annealed in the magnetic field of 6000 Oe and in dc electric field of 300 kV/m [23] whereas no annealing fields were required for $CrO_2$. The data on $Cr_2O_3$ are multiplied by a factor of 10 so as to compare its temperature variation with that measured on granular $CrO_2$. This comparison reveals that in both cases the ME signal changes sign at about 100 K. However, unlike what is observed in pure $Cr_2O_3$, the ME moments in granular $CrO_2$ do not vanish at the $T_N$ of $Cr_2O_3$, but continue to rise further till the measured temperature of 350K. Fig. 3c shows that the resultant moment exhibits a linear variation as a function of the applied- electric-field amplitude measured at a fixed temperature, as is expected for linear ME effects, typically seen in pure $Cr_2O_3$.

We first focus our attention to the change of sign in ME moments at about 100 K. It is to be noted that the sign of the induced moments for such measurements is arbitrary, but is fixed for a particular connection during a run. Therefore, the change of sign during one set of run is not arbitrary. It is recalled that the ME susceptibility measured on pure $Cr_2O_3$ shows a similar change of sign at around 100 K, which is well documented in literature [16, 19, 23]. This feature in pure $Cr_2O_3$ is understood to arise from an interplay between a two-ion term (electrically induced change in the exchange interactions in sublattices that disturbs the mutual compensation of antiparallel spins) and a single-ion term (due to the electric field induced g-shift) which have opposite signs. Although $Cr_2O_3$ appears only as grain boundary in granular $CrO_2$, both of them, granular $CrO_2$ and pure $Cr_2O_3$ exhibit a change of sign in the ME susceptibility, occurring in a similar temperature range and this feature is indicatative of strong interface effects. This provides compelling evidence that the ME response in granular $CrO_2$ is modulated by features intrinsic to the pure $Cr_2O_3$ phase.

We also observe that the ME signal is much larger in magnitude in relatively small applied electric field in $CrO_2$ and no magnetoelectric annealing is required as in case of $Cr_2O_3$. A rough attempt to extract the size of the corresponding magnetoelectric coupling for $CrO_2$ yields $\alpha$ ($\approx \mu_0 M_z/\mathrm{E}_z$) in the order of $10^{-7}$ s/m. This estimation is based on the experimentally observed electric field induced moment (m') and secondary effects such as the anisotropy of the ME effect, AFM domains and the polycrystalline nature of our sample have been neglected. This value is about 5 orders of magnitude larger than the maximal value of $\alpha$ for the pure $Cr_2O_3$ which exhibits $\alpha_{zz} \approx 4$ ps/m [16, 17, 23]. However, we emphasize that any comparison of $\alpha$ e.g. for the two samples studied at hand, should be taken very cautiously.

In this context, it is important to recall that while $Cr_2O_3$ is insulating, granular $CrO_2$ shows activated transport with relatively low resistivity values of the order of a few Ωcm [25, 26]. This may lead to additional contributions to the ME effect and need to be distinguished from the classical ME effects intrinsic to pure $Cr_2O_3$. For instance, the low resistivity of our samples may lead to generation of moments induced due to the surface currents, which we refer to as the Oersted moment, to differentiate it from ME response. During a ME measurement at a constant current amplitude, this contribution should be independent of the temperature - if we ignore the modulations driven by the ferromagnetic interactions.

In order to investigate the possible effect of Oersted moments, we conducted an experiment in the same configuration on a graphite sample. This sample consists of thin graphite sheets, commercially available from Goodfellow and three such sheets were glued together by silver paste so that the resistivity of this sample is of the order of a few Ωcm, similar to the $CrO_2$ sample. The sample geometry was similar to the $CrO_2$ sample, too. In Fig. 4, we compare the normalized electric field induced moments as observed in a cooling cycle for both the granular $CrO_2$ ($i_0 = 125$ μA= const) and the graphite sample ($i_0 = 175$ μA= const). The data indeed imply the presence of finite Oersted moments in the graphite model sample. However, the observed moments in the graphite sample show no change of sign and they are temperature independent. This is unlike what is observed in granular $CrO_2$. Thus, although Oersted moments may affect the magnitude of the observed signal, these contributions cannot explain the strong temperature dependence of the electric-field-induced moments as is seen in granular $CrO_2$.

We also note that it is nontrivial to estimate the magnitude of surface currents in our sample with randomly orientated grains with insulating grain boundary. Though we have tried to estimate the maximal possible magnitude of ME moments, taking into account the $Cr_2O_3$ surface layer outside the grains [1]. These calculations show that the magnitude of the ME moments is still 4 to 5 orders of magnitude smaller than what is observed experimentally and therefore the exact scenario cannot be understood unless interface effects are taken into accout.

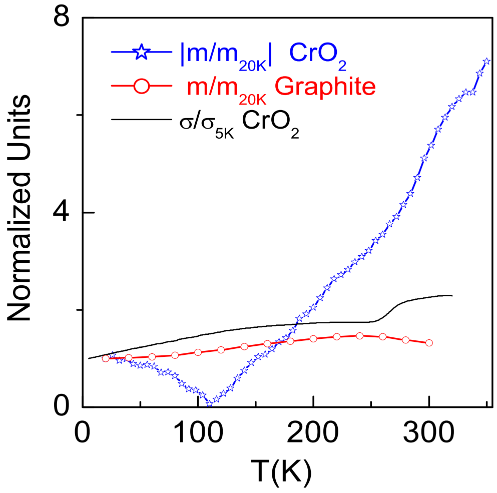

Fig. 4: Comparison of normalized values of electric field induced moment recorded in cooling cycle for $CrO_2$ sample (blue stars) and a graphite sheet (red circles) having resistivity in similar range with that of $CrO_2$ sample. The black line is the normalized conductance of $CrO_2$ measured in the bias current of 100 μA.

We also plot the normalized conductance measured at a fixed bias current of 100 μA for granular $CrO_2$ in the same graph (Fig. 4). This comparison reveals that the functional form of the observed moments in granular $CrO_2$ is strikingly different from what is expected from the surface currents associated to the Oersted moment. The observation of change of sign was also reconfirmed by measurements repeated in both constant current amplitude (Fig. 4, $i_0 = 125$ μA) and constant-voltage-amplitude mode (not shown). These experimental observations strongly indicate that the origin of electric-field-incuced moments in our sample is correlated with ME effects in $Cr_2O_3$.

While change of sign as well as linear variation of moments as a function of electric field (Figure 3c) point towards the modulation driven by AFM/ME $Cr_2O_3$, the continuous increase of the moment as a function of temperature right up to 350 K is puzzling. This is contrary to what is seen in the pure $Cr_2O_3$ phase where the ME moment vanishes at $T_N$ of $Cr_2O_3$ (307 K). Though such effects are not uncommon and plenty of work - particularly in tailor made FM/AFM systems - reports unusual exchange bias effects that exist beyond the Néel temperature of its AFM component [31–33]. These features are usually attributed to strain or proximity effect and we also have seen some manifestations in our samples [34]. However, the exact physical mechanisms that leads to such observation are not well explored.

In this context, it is recalled that in general, the microscopic origin of ME effects is understood to arise from four basic mechanisms such as g tensor, single ion anisotropy, symmetric and antisymmetric exchange mechanism [35,36]. Depending on the strength of interaction, the total ME effect is governed by one of these mechanisms or their combinations. For instance, the two-ion contribution, related to a net change in the bulk magnetization of AFM , arising due to the inequivalence of the two sublattices on application of the electric field, vanishes above the Néel temperature. However, the ME annealing effects as observed in pure $Cr_2O_3$ are explained in terms of the atomic single-ion ME coefficients which exist in the paramagnetic regime (i.e. above 307 K) in $Cr_2O_3$ but this effect is enhanced when long-range AFM order sets in [21]. The usual ME effect (related to the AFM order) is itself a weak effect and to observe the change due to individual moments is even more challenging. However, it is in principle possible to observe the ME effect related to the change in the magnitude of an individual moment on application of the electric field [35,36].

---

[1] Under assumptions that the $CrO_2$ sample consists of spherical grains with average diameter of 5μm and with grain boundaries layer of 2 nm $Cr_2O_3$, the electric field drop at the grain interface is about $10^3$ times the external electric field. As the volume ratio of $Cr_2O_3$ outside a single grain is about $10^{-3}$, the total electrically induced moment is finally the same as in the case of 100% $Cr_2O_3$.

In our case, the $Cr_2O_3$ appears at the interface of another long-range ordered magnet ($CrO_2$), whose $T_C$ is about 400 K. In this situation, the ME moments arising due to single-ion ME coefficients of $Cr_2O_3$ may still be finite above $T_N$, due to proximity effects [28,29]. Though we could measure the ME moments up to about 350 K, we speculate that they may eventually diminish only above 400K. Prior experimental data on thin films of $CrO_2$ having a surface layer of $Cr_2O_3$ as well as bilayers of $CrO_2/Cr_2O_3$ have also shown some interesting interface effects [29,30].

This study indicates that it is important to explore the influence of the AFM/ME character of $Cr_2O_3$ when it appears at the interface, particularly in transport measurements. In these samples, we do see unusual thermal history and bias current effects in resistivity measurements (unpublished). These data also point towards the need to take into account the ME character of the grain boundary in order to understnd the transport mechanism in this system.

In conclusion, from direct measurement of high-resolution transmission electron microscopy we show that our $CrO_2$ grains contain a surface layer of *polycrystalline* $Cr_2O_3$. This can account for the much improved tunneling magnetoresistance as has earlier been observed in these samples. The influence of the magnetoelectric character of the surface layer is visible in magnetoelectric susceptibility measurements. The observation of finite electric-field-induced moments right up to 350K in granular $CrO_2$ can be understood to arise from interface effects, taking into account the modulations driven by the ME character of $Cr_2O_3$. A finite ME susceptibility at room temperature may prove to be useful in $CrO_2$ based devices.

* * *

A.B. acknowledges support through a EU Marie Curie IIF fellowship under project 040127-NEWMATCR. P.B. acknowledges support by the DFG through SFB 491. Part of the work was funded by the DFG (HE 3439/6)

## REFERENCES

[1] S-W. Cheong and M. Mostovoy, *Nat. Mater.*, **6** (2007) 13.
[2] R. Ramesh and N. A. Spaldin , *Nat. Mater.*, **6** (2007) 21.
[3] M. Fiebig, *J. Phys. D: Appl.Phys.*, **38** (2005) R123.
[4] K. Dörr , *J. Phys. D: Appl.Phys.*, **39** (2006) R125.
[5] H.Y. Hwang and S-W. Cheong, *Science*, **278** (1997) 1607.
[6] R.A. Groot et al., *Phys. Rev. Lett.*, **50** (1983) 2024.
[7] R.J. Soulen et al., *Science*, **282** (1998) 85.
[8] J. S. Parker, S. M. Watts, P. G. Ivanov and P. Xiong, *Phys. Rev. Lett.*, **88** (2001) 196601.
[9] L. Spinu, H. Srikanth, A.Gupta, X.W. Li and Gang Xiao, *Phy. Rev. B*, **62** (2000) 8931.
[10] P.G. Ivanov, S.M. Watts and D.M.Lind, *J.Appl. Phys.*, **89** (2001) 1035.
[11] U. Ruediger et al.,, *J.Appl. Phys.*, **89** (2001) 7699.
[12] P.G. Ivanov and K.M. Bussmann, *J. Appl. Phys.*, **105** (2007) 07B107.
[13] J.M.D Coey et al., *Phys. Rev. Lett.*, **80** (1998) 3815.
[14] J. Dai et al., *Appl. Phys. Lett.*, **77** (() 2000)2840.
[15] J. Dai and J. Tang, *Appl. Phys. Lett*, **63** (2001) 064410.
[16] G.T. Rado and V.J. Folen, *Phys. Rev. Lett.*, **7** (1961) 310.
[17] D.N.Astrov, *Sov. Phys. JETP*, **11** (1960) 708.
[18] V.J. Folen, G.T. Rado and E.W. Stalder., *Phys. Rev. Lett.*, **6** (1961) 607.
[19] R. Hornreich and S.Shtrikman, *Phys. Rev.*, **161** (1961) 506.
[20] S. Shtrikman and D. Treves, *Phys. Rev.*, **130** (1963) 986.
[21] T.J. Martin and J.C. Anderson, *Phys. Lett.*, **11** (1964) 109.
[22] P.J. Brown et al., *J. Phys.: Cond. Matter*, **10** (1998) 663.
[23] P. Borisov et al., *Rev. Sci. Instrum.*, **78** (2007) 106105.
[24] A Bajpai and A.K. Nigam , *US Patent* , **7276226** ( ) .
[25] A. Bajpai and A.K. Nigam , *Phys. Rev. B*, **75** (2007) 064403.
[26] A. Bajpai and A.K. Nigam, *J. Appl. Phys.*, **101** (2007) 10391.
[27] J. Thomas and T. Gemming, *Springer, ISBN 978-3-540-85301-5*, **2008** (231) .
[28] Y. Song, A.L. Schmitt and Song Jin , *Nano Lett.*, **8** (2008) 2356.
[29] Cheng R. et al., *Phys. Lett.* , **A302** (2008) 21.
[30] N.A. Frey et al., *Phys. Rev. B* , **74** (2006) 024420.
[31] S. Sahoo et al., *Appl. Phys. Lett.*, **91** (2007) 172506.
[32] H. Shi et al., *Phys. Rev. B*, **69** (2004) 214416.
[33] P.J. Van der Zaag et al., *Phys. Rev. Lett*, **84** (2000) 6102.
[34] A. Bajpai et al., *J. Phys: Condens Matter*, **22** (2010) 096005.
[35] O.F. de Alcantara Bonfim and G.A. Gehring, *Adv. Phys.*, **29** (1980) 731.
[36] G.A. Gehring, *Ferroelectrics*, **161** (1993) 275.